Experimental Mechanics (2019) 59:991–1005
https://doi.org/10.1007/s11340-019-00512-4

Effect of Fragile Speckle Patterns on Accuracy of Digital Volume Correlation

B.P. Croom [1] · H. Jin [2] · B. Mills [2] · X. Li [1]

Received: 13 September 2018 / Accepted: 5 April 2019 / Published online: 30 April 2019

Abstract

Due to challenges in generating high-quality 3D speckle patterns for Digital Volume Correlation (DVC) strain measurements, DVC experiments often utilize the intrinsic texture and contrast of composite microstructures. One common deficiency of these natural speckle patterns is their poor durability under large deformations, which can lead to decorrelation and inaccurate strain measurements. Using syntactic foams as a model material, the effects of speckle pattern degradation on the accuracy of DVC displacement and strain measurements are assessed with both experimentally-acquired and numerically-generated images. It is shown that measurement error can be classified into two regimes as a function of the percentage of markers that have disappeared from the speckle pattern. For minor levels of damage beneath a critical level of damage, displacement and strain error remained near the noise floor of less than 0.05 *voxels* and 100 $\mu\varepsilon$, respectively; above this level, error rapidly increased to unacceptable levels above 0.2 voxels and 10,000 $\mu\varepsilon$. This transition occurred after 30%–40% of the speckles disappeared, depending on characteristics of the speckle pattern and its degradation mechanisms. These results suggest that accurate DVC measurements can be obtained in many types of fragile materials despite severe damage to the speckle pattern.

Keywords Digital volume correlation · Error assessment · Syntactic foams · Decorrelation · Speckle pattern

Introduction

Both digital image correlation (DIC) [1] and its three-dimensional analogue digital volume correlation (DVC) [2] compute the deformation field by tracking the aggregate motion of neighborhoods of features through a sequence of *in situ* experimental images (or 3D tomograms acquired by volumetric imaging techniques). This is achieved by correlating the deformed image with the original undeformed image, and computing the translation, rotation and deformation of the image from the reference state into the deformed state. Generally speaking, the sample should exhibit a high-quality, high-contrast, random "speckle pattern" to ensure the uniqueness and accuracy of the deformation measurement [3, 4]. One of the fundamental assumptions of DIC and DVC algorithms is that the individual speckles in the pattern be ***durable*** to allow them to be tracked in each image, so they should not substantially change appearance or disappear throughout the experiment. While such a speckle pattern can readily be applied to the surface of a specimen using spray paint, toner, or one of many other techniques for two-dimensional or stereo DIC, it is intrinsically challenging (and often undesirable) to modify the internal microstructure of three-dimensional specimens to meet these criteria for DVC measurement [5]. Instead, the intrinsic contrast and texture of the microstructure can substitute for a high-quality artificial pattern.

As a result, a common deficiency of volumetric speckle patterns is the degradation of the microstructure under load, which can lead to decorrelation and inaccurate measurements. One common example is due to the development of damage in the material, which introduces new contrasting features to the material that were not present in the reference state. This is frequently encountered in

✉ H. Jin
hjin@sandia.gov

✉ X. Li
xl3p@virginia.edu

[1] Department of Mechanical and Aerospace Engineering, University of Virginia, 122 Engineer's Way, Charlottesville, VA 22904, USA

[2] Sandia National Laboratories, P.O. Box 969, Livermore, CA 94551, USA

brittle materials that undergo microcracking, such as ceramic matrix composites [6–9], plasterboard [10], and graphite [11]. Alternatively, this can be observed in the rupture of ductile metals, which is commonly preceded by void initiation, coalescence and growth into a crack [12]. Unless the damage mechanisms are explicitly incorporated into the warping functions for the DVC algorithms (such as Heaviside DVC [13] or extended-DVC analogous to X-FEM techniques [14]), these features cause the image to violate the principle of "gray-level conservation" and therefore reduce the quality of the DVC measurement. However, it is generally acknowledged that DVC measurements will remain reasonably accurate provided the volume of damaged material remains small compared to the quantity of markers in the speckle pattern, as is the case in these examples.

Another scenario is the disappearance of individual speckles between the reference and deformed states, which also deleteriously affects DVC accuracy. This is particularly relevant for DVC experiments that tend to rely on the intrinsic texture of the material of interest, which may not be stable at large deformation as in the cases of foams [15–17], bone [2, 18] and granular materials [19, 20]. Even in surface-based DIC applications where artificial patterns are easily applied, the pattern may degrade when painted markers flake off the area of interest or fade with large deformation. It is currently unclear how this degradation affects DVC accuracy.

Recent *in situ* X-ray Computed Tomography (XCT) experimental measurements by the authors have shown that DVC remains viable even in cases of severe damage to the speckle pattern with only minor losses in accuracy. As reported in Ref. [21], tomograms of syntactic foams were acquired at increasing levels of uniaxial compression. The syntactic foam consisted of an elastomer matrix filled with hollow glass microballoons (GMBs), which produced an archetypal 3D speckle pattern in the undamaged state (Fig. 1(a)). At increasing deformation, many of these GMBs crushed under mechanical load and eventually disappeared from the tomogram (Fig. 1(b)), so a significant fraction of the markers that constituted the speckle pattern eventually disappeared from the images. Remarkably, accurate DVC measurements were obtained until 40% of the GMBs had collapsed.

The ability to accurately correlate heavily damaged tomograms challenges our current assumptions about requirements for speckle patterns. In particular, these findings indicate that rules about gray level conservation can be relaxed in certain cases to permit measurement of specimens with fragile speckle patterns. The objective of this paper is to explore the limits of DVC for materials with fragile microstructures and speckle patterns, and to quantify the effects of microstructure degradation as well as DVC analysis parameters on measurement accuracy. Certainly, use of DVC to study fragile microstructure comes at a cost of decreased accuracy, but how much damage is tolerable? The feasibility of DVC in these scenarios is first explored through experimental measurements using rigid body motion experiments to capture the effect on error under real imaging conditions. Later, analysis of synthetic images with controlled levels of speckle pattern degradation is used to more accurately quantify the effects on DVC accuracy. Finally, these effects are addressed from a theoretical perspective to reconcile these trends with existing models of DIC error.

DVC Preliminaries

The basis for all DVC algorithms is the cross-correlation between the reference and deformed subvolumes. Since cross-correlation measures the similarity between two volumes, the optimal solution is obtained when each pixel in the deformed volume is mapped to the corresponding pixel in the reference coordinate, *i.e.* the displacement field is solved. One way of achieving this is by using optimization schemes to maximize the zero-mean, normalized cross-correlation (ZNCC), which is notably insensitive to systematic changes in contrast and illumination [3]. The ZNCC is computed as,

$$C_{ZNCC}(\boldsymbol{x}) = \frac{1}{N}\sum_{\boldsymbol{x}\in S}\left(\frac{F(\boldsymbol{x})-\overline{F}}{\sigma_F}\ \frac{G(\boldsymbol{x}+\boldsymbol{u}(\boldsymbol{x}))-\overline{G}}{\sigma_G}\right) \tag{1}$$

where F and G correspond to the reference and deformed images, $\boldsymbol{x}$ represents the coordinates within the reference subset S, $\boldsymbol{u}(\boldsymbol{x})$ is the displacement field that maps undeformed coordinates into their deformed state, $\overline{F}$ and $\overline{G}$ indicate the average intensities of each subset, and σ_F and σ_G are the standard deviations of intensities within each subset. A high correlation score $C_{ZNCC} \to 1$ would indicate a strong match between the two specimens, implying that the physical displacement field has been accurately measured. The strain field can then be obtained through the spatial derivatives of $\boldsymbol{u}(\boldsymbol{x})$.

Notation to Describe Specimen Degradation

The primary concern about correlating images of fragile speckle patterns is that C_{ZNCC} will decrease as the specimen degrades, increasing the possibility that the optimization algorithm will identify inaccurate displacement and strain fields due to decorrelation effects. For purposes of this paper, unique notation is developed to concisely describe the damaged character of speckle patterns:

- ϕ – Volume fraction of markers in undamaged state (from 0 to 1)
- α – Fraction of markers that are damaged (from 0 to 1)
- C – Residual contrast of all damaged markers (from 0 to 1)

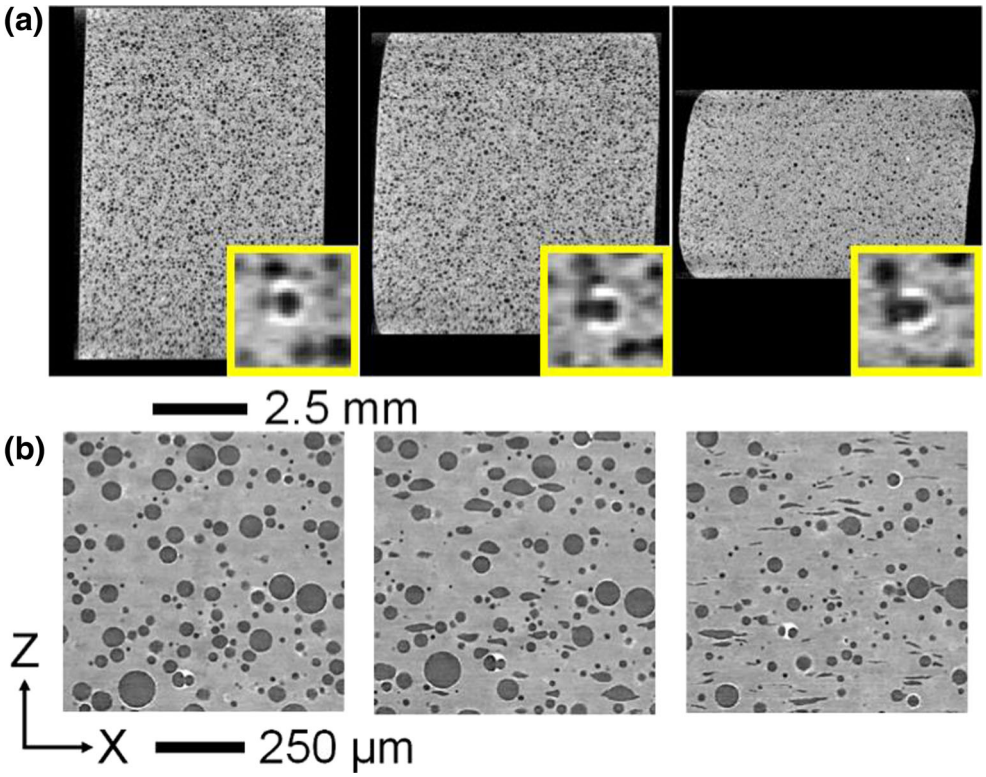

Fig. 1 Virtual cross-sections of compressed syntactic foam during in situ experiment. (a) Slices from low-resolution for DVC analysis at increasing strain, with insets showing subvolume size. (b) Slices from the corresponding high-resolution XCT images, showing collapse of GMBs. Images adapted from experiment in Ref. [21]

Experimental Methods

Materials

Sylgard GMB specimens were prepared by mixing A16 glass microballoons (3 M) into two-part Sylgard 184 silicone elastomer (Dow Corning) and curing agent. The mixture was drawn into a cylindrical syringe and cured at room temperature with an accelerator. After curing, the molded foam was carefully cut into cylindrical specimens with 7 mm height and diameters of 4.8 mm. The diameter of A16 GMBs ranges from 30 to 95 μm within 10–90% distribution, with a mean diameter of 60 μm. Three specimens were manufactured with nominal GMB volume fractions of 0.20, 0.30 and 0.46. Since the low-resolution tomograms could not discern GMB walls from the matrix, the actual void volume fractions were 0.147, 0.225 and 0.422; to allow generalization to other types of speckle patterns, all results are reported in terms of the void volume fraction.

Rigid Body Motion Experiments

Experimental assessment of the error due to fragile specimens was performed using rigid body motion experiments during *in situ* compression of the syntactic foams. Syntactic foam specimens were compressed uniaxially using a custom, screw-driven loading stage as reported in [6, 22]. The specimen was deformed between two acrylic platens to minimize reconstruction artifacts near the specimen edges. Each specimen was compressed in roughly 500 μm increments until DVC failed to achieve correlation, resulting in 5 or 6 *in situ* load steps per specimen.

Three tomograms were acquired at each load step. First, one high-resolution tomogram with voxel resolution of $[1.7\ \mu m]^3$ was used to quantify the volume fraction of GMBs in the undamaged state, and the fraction of damaged GMBs in subsequent steps. Second, a low-resolution tomogram was acquired with voxel resolution of $[8.5\ \mu m]^3$, resulting in a typical speckle diameter of 6–8 voxels that was ideal for DVC analysis. Finally, an additional low-resolution tomogram was acquired after axially displacing the sample 250 μm. The higher resolution tomogram was necessary to accurately measure the size and Feret shape (3D aspect ratio) of the GMBs [23], while the difference in measured displacements and strains between the pair of low-resolution tomograms enabled an assessment of DVC error. All tomographic imaging was performed using X-radia MicroXCT 200 with X-ray source parameters 80 keV and 8 W. High-resolution tomograms were reconstructed from a set of 2401 radiographs between −103° and 103° rotation with 6.5 s exposure, and the low-resolution tomograms were reconstructed from a set of 1401 radiographs between −103° and 103° rotation with 7 s exposure.

Dimensional quantification of the GMBs was performed using Python image processing scripts and Avizo Fire 9.0. The raw 16-bit high-resolution tomograms were sequentially

smoothed using nonlocal means filters, downsampled to 8-bit images, thresholded and segmented with standard image processing techniques. The 3D Feret shape (FS, equivalent to the particle's aspect ratio) was used to identify the collapse of each segmented GMB, where FS > 1.3 indicated an ellipsoidal geometry consistent with GMB collapse. In contrast, low FS indicated spherical geometry of an intact GMB.

Both the mechanical response and the damage behavior are reported in Fig. 2 for the three different volume fractions. The stress-strain curves were typical for elastomeric syntactic foams [24], which generally exhibit an initially stiff elastic response, a plateau region associated with GMB collapse at relatively constant stress, and densification of the foam [25]. Both the elastic stiffness and prominence of the plateau region increased with higher GMB reinforcement, whereas the syntactic foams with lower GMB volume fraction behaved more like the elastomer matrix. In the three specimens, appreciable GMB collapse occurred only after reaching the plateau region, and damage increased approximately linearly thereafter. GMB collapse occurred more rapidly at higher volume fractions, as particle clustering is known to amplify the GMB stresses [21, 26, 27].

The low-resolution tomograms were independently correlated against a single reference tomogram using commercial DVC code (Vic-Volume, Correlated Solutions) with a subset size of 29 voxels, and step size of 10 voxels. This subset size was selected to include roughly $3^3 = 27$ speckles per subset for the $\phi = 0.147$ specimen, which is a general guideline for DIC/DVC analysis. A sensitivity study found that step size had no effect on the displacement errors. Additionally, the step size did not affect the nonlinear dependence between strain error and damage, but simply scaled the error by a factor of $1/step^2$; the latter relationship matches the sensitivity of a central-differences numerical differentiation scheme to noise.

Strain was computed with a strain filter size of 5 subsets, which was the minimum filter size available in the software. The strain filter averaged the displacement gradient uniformly across neighboring subsets, with the aim of decreasing measurement noise compared to calculation of strain from a single subset. As the objective of this analysis was to identify the "worst case" DVC strain error due to speckle pattern degradation, the total strain filtering was adjusted to the minimum possible value in the software; future users could increase strain filtering to further reduce the effects of speckle pattern degradation at the cost of spatial resolution. This combination of analysis parameters resulted in a virtual strain gage size of $[79 \text{ voxels}]^3 = [672\ \mu\text{m}]^3$. All analysis was performed with a 4-tap spline-based interpolation scheme [3]. To measure the error in the DVC-computed strain, the difference in measured strain was recorded at each subset for the corresponding deformed and deformed rigid body motion tomograms.

Experimental Results

To experimentally evaluate the displacement and strain errors, the DVC measurements were compared before and after rigid body motion. Since both tomograms were acquired at the same state of compression and were correlated independently against the same reference tomogram, they should theoretically exhibit the same strain field. Any differences are attributed to the various sources of measurement error. In particular, error in the undeformed state ($\varepsilon = 0$) reflects the noise floor of the measurement system, while subsequent increases in error as the syntactic foam is compressed can be attributed to the effects of speckle pattern degradation.

Displacement Error

The axial displacement field for a syntactic foam specimen with void volume fraction $\phi = 0.225$ is presented in Fig. 3 at three increasing deformations. While the specimen exhibited some

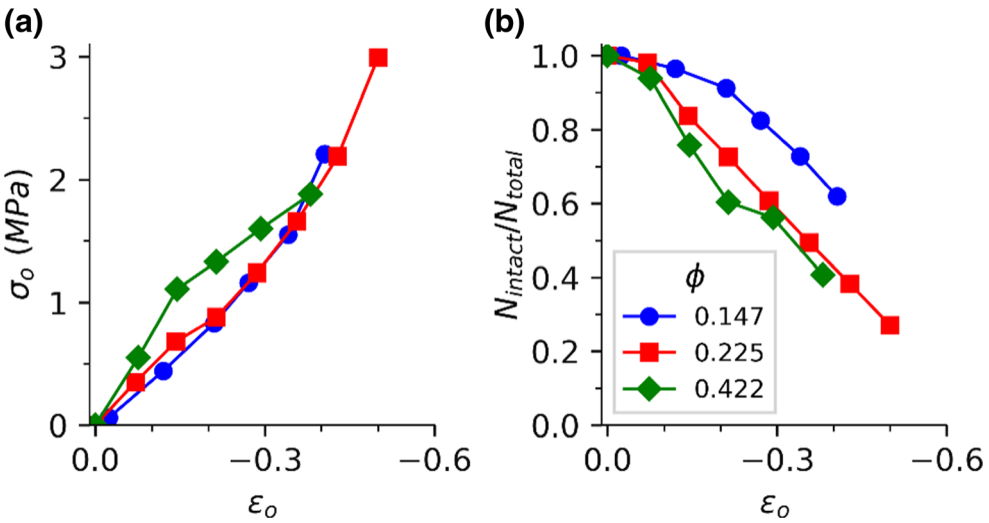

Fig. 2 Mechanical behavior of syntactic foam specimens. (a) Engineering stress vs. engineering strain curves. (b) Fraction of intact specimens vs. engineering strain

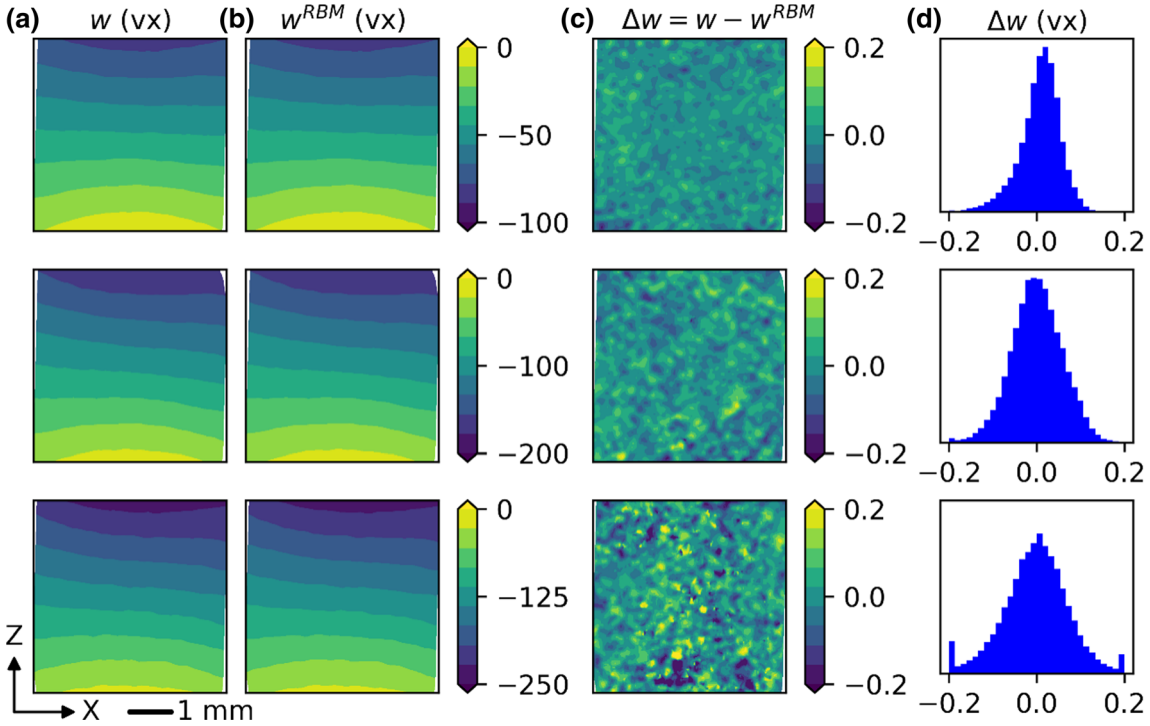

Fig. 3 Experimental assessment of axial displacement error for syntactic foam specimen with $\phi = 0.223$. (a-b) Measured axial displacement in voxels (a) before (w) and (b) after rigid body motion (w^{RBM}); (c) difference between measured displacements Δw; and (d) histogram of Δw. Results are shown at (top) nominal strain $\varepsilon_0 = -0.12$, (middle) $\varepsilon_o = -0.24$, and (bottom) $\varepsilon_0 = -0.30$. Note that the rigid body motion is removed when plotting w^{RBM}

buckling at the highest loads, the displacement field was predominantly uniaxial in nature (Fig. 3(a)). After removing rigid body motion from the measurements, it was clear that the DVC measurements exhibited strong repeatability (Fig. 3(b)). Any differences in the experimental displacement fields were imperceptible at this level of contrast, even at the largest deformations.

To highlight any discrepancy between the two sets of DVC measurements, Fig. 3(c) shows the difference in measured axial displacement $\Delta w = w - w^{RBM}$ at the same three deformations. For nominal strains of strain $\varepsilon_0 = -0.12$ and $\varepsilon_o = -0.24$, the resulting DVC error was small in magnitude. For all subsets the error remained below 0.2 voxels, and in most cases was below .05 voxels. As confirmed in Fig. 3(d), the displacement error was only marginally higher at $\varepsilon_o = -0.24$ compared to $\varepsilon_o = -0.12$. Additionally, variation in Δw was uniform and random throughout the specimen, indicating that the error calculation was not affected by distortion artifacts or damage localization.

However, at the final strain increment of $\varepsilon_0 = -0.30$, the error noticeably increased throughout the specimen. Inspection of Fig. 3(c) for this deformation identified several anomalous "hot spots" in the displacement calculation, indicating large discrepancy of $\Delta w > 0.2$ voxels between the w and w^{RBM} calculations at these points. Despite this, the majority of the displacement measurements remained accurate to within $\Delta w < 0.1$ voxels, indicating that the DVC analysis was generally trustworthy despite severe degradation to the speckle pattern. Thus, DVC may cautiously be used in specimens despite widespread microstructural damage.

This analysis was repeated on the additional two specimens to compare the error trends as a function of the syntactic foam microstructure and damage characteristics (Fig. 4). These results loosely identify two key analysis regimes. First, DVC error remained near the noise floor below a critical level of speckle pattern degradation. These errors were approximately $\Delta w = 0.03$ voxels for $\phi = 0.225$ and 0.422, and $\Delta w = 0.05$ for $\phi = 0.147$. In this regime, DVC measurements could be considered "stable," and good accuracy can be guaranteed.

Second, after exceeding a critical level of speckle pattern degradation at $\alpha \approx 0.3$, the displacement error rapidly increased. In other words, the effects of minor speckle pattern degradation on DVC accuracy were less significant than other experimental factors, including the initial speckle pattern quality or imaging noise. Only at severe degradation did this error source become significant. Thus, these measurements became "unstable," where accuracy depended on the local damage state and cannot be generally guaranteed.

Strain Error

Equivalent analyses were performed to interpret the effects of speckle pattern degradation on strain measurement accuracy. First, the axial strain fields are presented in Fig. 5(a). Under uniform axial compression, the specimen exhibited strong

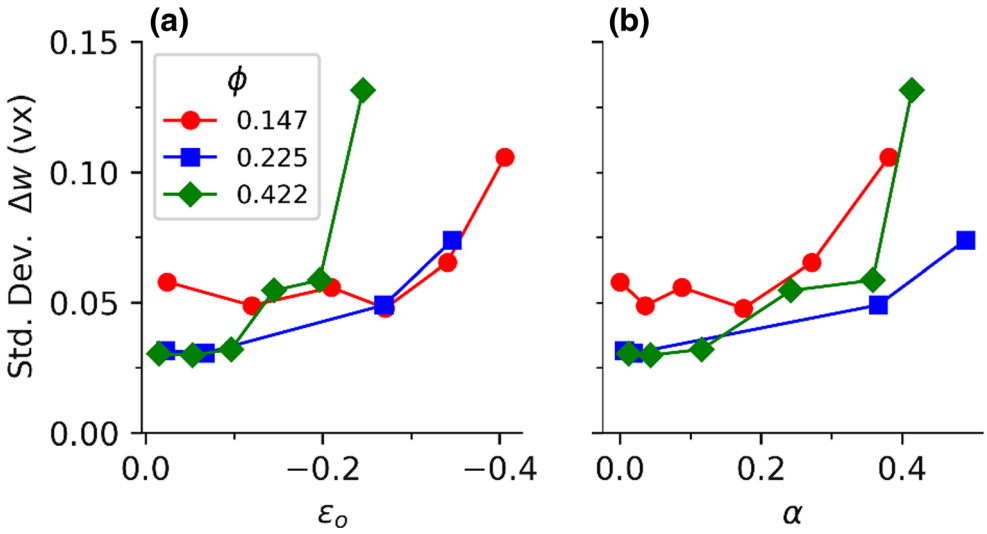

Fig. 4 Displacement error as function of (a) engineering strain ε_o and (b) fraction of damaged GMBs α in the different syntactic foams

variation in axial strain due to heterogeneous collapse of GMBs. As was previously discussed in [21] and also observed in some other syntactic foams [28], this behavior was mechanistically related to the redistribution of stress around collapsed GMBs and the propagation of damage through the syntactic foam. For the specimen with void volume fraction $\phi = 0.225$, the intensity of the strain field variation increased from $\varepsilon_{zz} \approx 0.01$ at a nominal strain of $\varepsilon_0 = -0.12$, to $\varepsilon_{zz} \approx 0.05$ at a nominal strain of $\varepsilon_0 = -0.30$. Analysis of the strains after rigid body motion (Fig. 5(b)) showed very little difference compared to the original analysis, confirming the measurement accuracy.

To more precisely evaluate the error, the difference between measured strain fields, $\Delta\varepsilon_{zz} = \varepsilon_{zz} - \varepsilon_{zz}^{RBM}$, was computed at each subvolume (Fig. 5(c)). Here, while the $\Delta\varepsilon_{zz}$ field exhibited a similar banded appearance, the magnitude of variation in $\Delta\varepsilon_{zz}$was roughly 5 times smaller than the variation in ε_{zz}. This trend was especially true when the specimen was imaged at low strain with little degradation to the speckle pattern ($\varepsilon_o = -0.12$). In the low-strain images, variation

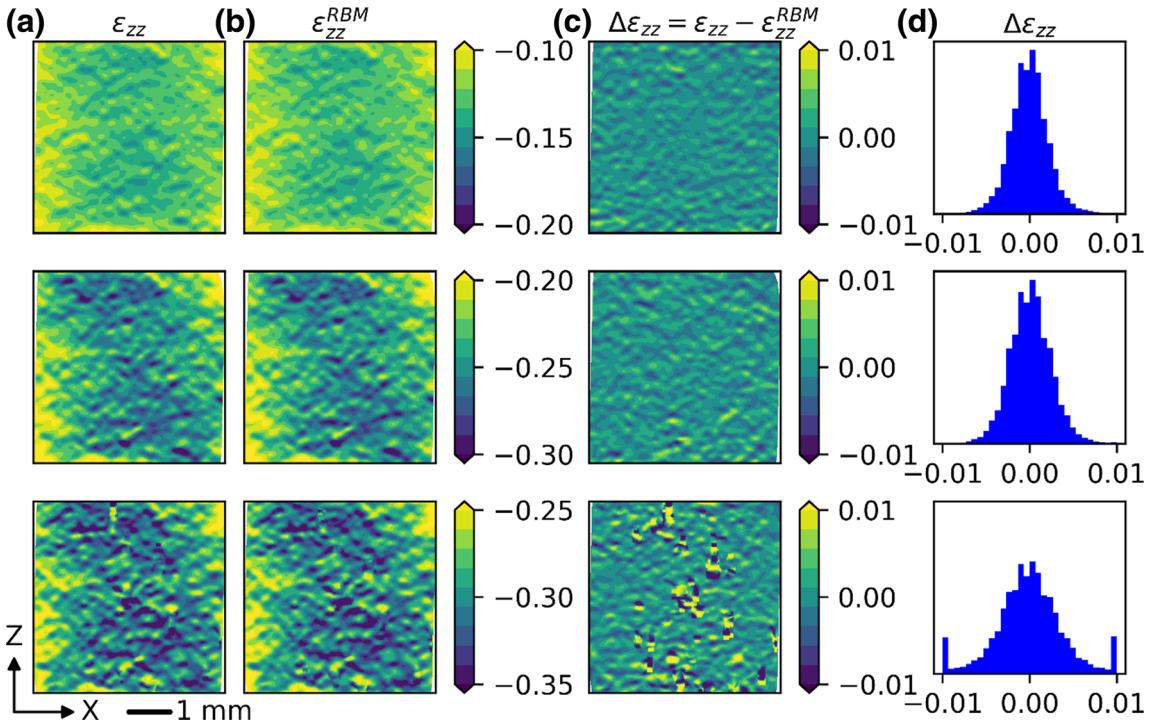

Fig. 5 Experimental assessment of strain error for syntactic foam specimen with $\phi = 0.223$. (a-b) Measured axial strain (a) before and (b) after rigid body motion; (c) difference between measured strain $\Delta\varepsilon_{zz}$; and (d) histogram of $\Delta\varepsilon_{zz}$. Results are shown at (top) nominal strain $\varepsilon_0 = -0.12$, (middle) $\varepsilon_o = -0.24$, and (bottom) $\varepsilon_0 = -0.30$

approached the noise floor associated with this particular combination of XCT imaging and DVC analysis parameters. At higher strains ($\varepsilon_o = -0.30$) with more damage, the error increased marginally, although many subvolumes produced obviously spurious strain values with $|\Delta\varepsilon_{zz}| > 0.01$; these points appeared as yellow or purple spots in Fig. 5(c). This trend was validated by comparing the histograms of $\Delta\varepsilon_{zz}$ in Fig. 5(d), which showed both an increase in both standard deviation and number of outliers in each measured strain field. Interestingly, the increase in strain error occurred rapidly, as error at an intermediate strain of $\varepsilon_o = -0.24$ remained small.

Similar analyses were repeated for all three specimens, and the standard deviation of $\Delta\varepsilon_{zz}$ as a function of the speckle pattern degradation is reported for each load increment in Fig. 6. These trends resembled those for displacement in Fig. 4, and also showed that the accuracy of the DVC strain measurements remained near the measurement noise floor until a critical level of speckle pattern degradation was achieved. Typical error in this regime of minor speckle pattern degradation ranged from $\sigma_{\Delta\varepsilon_{zz}} = 98\ \mu\varepsilon$ for $\phi = 0.147$ and 54 $\mu\varepsilon$ for $\phi = 0.422$, with the different speckle pattern densities accounting for the discrepancies between specimens.

In contrast, error in the strain measurement rapidly grew to unacceptable levels once the speckle pattern degradation reached a critical value. This effect was much more prominent for strain than for displacement, which can be attributed to the sensitivity of numerical differentiation schemes (to compute strain) to noise in the displacement signal. Due to volume-fraction dependent damage mechanisms for the syntactic foams, this transition varied somewhat between specimens. This transition occurred most rapidly at $\varepsilon_o = -0.2$ in the high volume fraction specimen, and later at $\varepsilon_o = -0.35$ in the low volume fraction specimen.

When measured in terms of damage to the speckle pattern, the results suggested that the critical level of degradation varied with both the GMB content and the damage mechanisms in the syntactic foam. For instance, the low volume fraction specimen exhibited the least resilience to speckle pattern damage with critical $\alpha \approx 0.27$ before error rapidly increased, which could be attributed to the sparse speckle pattern. On the other hand, the two specimens with higher volume fractions exhibited a critical $\alpha \approx 0.36$, indicating the benefit of a denser speckle pattern. Despite this, error increased faster in the $\phi = 0.422$ specimen after the critical transition, possibly due to enhanced strain localization.

Numerical Methods

While the experimental results clearly showed that accurate DVC measurements could be obtained despite widespread damage to the speckle pattern, these trends were convoluted by imaging artifacts such as distortion and other XCT error sources [29]. Additionally, heterogeneous deformation such as crush-band effects or strain localization [28] could further bias these measurements.

To address these challenges, synthetic images were generated and then analyzed by DVC to assess the separate roles of *fraction of damaged markers* and *degraded marker contrast* on the accuracy of DVC strain computations. These two parameters can approximate the degradation of many other materials in addition to syntactic foams. For example, while GMBs tend to quickly collapse and disappear from tomograms, other materials may exhibit a more gradual failure process in which markers slowly lose contrast. Simulations were performed for many volume fractions of markers. In this way, the simulation results can be readily adapted to other material systems.

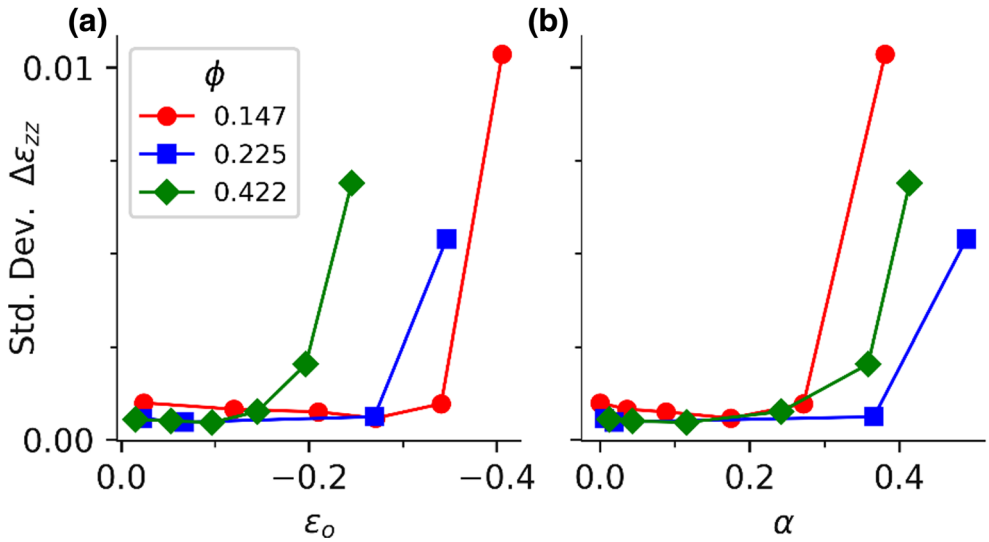

Fig. 6 Strain error as function of (a) engineering strain ε_o and (b) fraction of damaged GMBs α in the different syntactic foams

Generation of Synthetic Images

To establish the effects of pattern degradation on DVC error, artificial images with increasing levels of degradation and no strain were generated. Synthetic images with prescribed damage levels were developed through a three-step process of generating an undamaged reference pattern, degrading selected markers in the pattern, and then adding Gaussian noise to simulate experimental image conditions. Correlation of the synthetic volumes to the undamaged reference state using commercial DVC software provided an assessment of errors due to microstructure degradation.

First, a reference volume of size $1024 \times 256 \times 256$ voxels was generated with bright markers on a dark background by perturbing the position of markers on a 3D regular grid, similar to the technique used in [30]. The grid pitch was modified to change the volume fraction ϕ between 0.136 and 0.407 which encompassed representative porosities found in many syntactic foams and other DVC specimens [24, 28, 31, 32]. Speckles were modeled as modified 3D Gaussian signals with standard deviations σ randomly selected between 1 and 3 voxels,

$$I(\boldsymbol{x}) = \min\left(200, 400 exp\left(\sum_{i=1}^{3} \frac{-\left(x_i - x_i^c\right)^2}{\sigma^2}\right)\right) \tag{2}$$

where x_i represents the image coordinate, and x_i^c represents the subpixel center of the marker. The intensity of the central region in each speckle was truncated to imitate the uniform intensity of the hollow GMBs. In contrast to explicitly modeling the spherical particles, the modified Gaussian profile allowed facile imposition of subpixel displacements and deformations without relying on downsampling or interpolation filters. The speckles in the deformed images were analytically translated by 0.5 voxels from their reference position.

To efficiently survey the different combinations of α and C that represent various degrees of pattern degradation, damage was introduced to each pattern by randomly flagging markers for degradation as a linear function of the x coordinate. In this way, the probability of damage increased from $\alpha = 0.0$ at $x = 0$ to $\alpha = 1.0$ at $x = 1024$ (Fig. 7). The residual contrast of each flagged particle was incrementally decreased from $C = 1.0$ to 0.0, resulting in several images with many faint particles and one image with fully deleted particles. Since damage only varied in the x direction, there existed many data points on each $y-z$ plane to statistically analyze the effects of marker degradation. The intensities of the 3D volumes were scaled for 8-bit images, with the dark background assigned an intensity of 25, and the undamaged particles an intensity of 225; this intensity range allowed noise to be added to the image.

Finally, Gaussian noise was independently added to each image to approximate error in the imaging conditions. X-ray tomograms typically exhibit higher levels of noise than 2D optical images, and this noise will limit the accuracy of the strain computation. We quantify noise using the Noise to Signal Ratio (NSR), defined as

$$NSR = \frac{\sigma_{noise}}{I_{max} - I_{min}} \tag{3}$$

where σ_{noise} is the standard deviation of the noise, and $I_{max} - I_{min}$ is the intensity range in the signal. Our experimental results using laboratory-based XCT equipment yielded tomograms with NSR of ~3%, whereas tomograms from synchrotron or more modern XCT systems could produce lower noise levels. A sensitivity study found that error in strain computation due to NSR remained below 0.0001, which was insignificant relative to the effect of a fragile speckle pattern (with $\sigma_\varepsilon \approx 0.001 - 0.01$). Therefore, simulations were performed with a representative NSR of 3%.

DVC Analysis

DVC analysis was performed using the commercial VicVolume DVC software (Correlated Solutions) with parameters that matched the experimental error analysis (subset size of 29^3 voxels and step size of 10 voxels). These parameters resulted in ~50,000 subsets per volume, and 529 subsets for a given fraction of damaged markers. Strain measurement was again performed with a strain filter of size $[5]^3$ subsets, which was the minimum amount of filtering in the DVC software. Additional analyses were performed with a range of subset sizes to assess the sensitivity to this parameter.

Numerical Results

Effect of Speckle Pattern Degradation

Analysis of the zero-displacement simulations clearly revealed that the average marker volume fraction ϕ, the fraction of damaged markers α, and the residual contrast of damaged markers C strongly influenced the accuracy of the displacement computations, as summarized in Fig. 8. Results are presented for three different volume fractions that corresponded to those used in the experiments, and error is defined as the standard deviation of the measured artificial displacement.

Similar to the experimental results, there appeared to exist two domains for displacement computation. During the initial stable computation regime, the displacement error increased linearly with respect to α. This continued until a critical damage value was reached, after which the computation became unstable and error increased rapidly. Below the critical level of speckle pattern degradation, the error increased gradually with α but remained relatively small; in the worst-case scenario with $\phi = 0.137$ and $C = 0.0$, the error remained less than 0.2

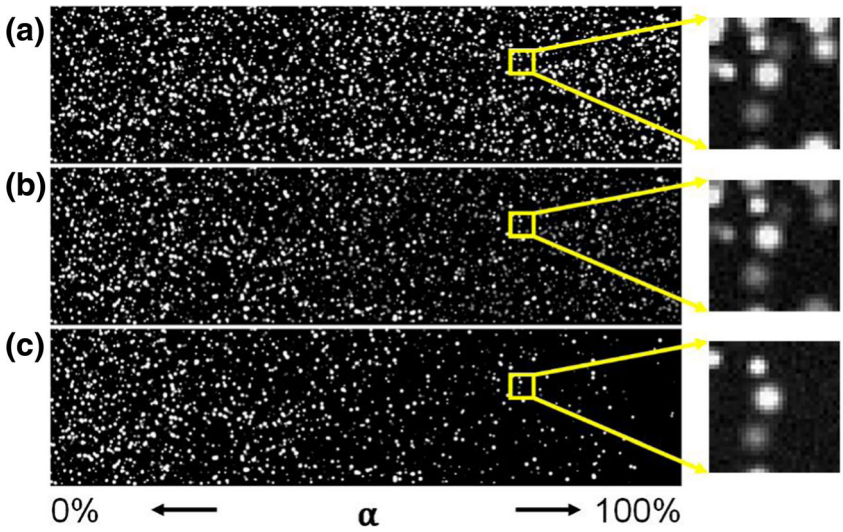

Fig. 7 Damage gradient in synthetic zero-strain images (a-c) Corresponding 2D slices with (a) $C = 1.0$, (b) $C = 0.5$, and (c) $C = 0.0$. Insets on right indicate subset size (29^3 voxels) used in DVC analysis, and highlight how selected markers gradually faded with decreasing C. $\phi = 0.137$

voxels throughout the stable DVC regime. The transition into the unstable regime is identified by the inflection point in the plots, which varied slightly with ϕ and C; values of this transition point (for $C = 0.0$) ranged from $\alpha = 0.62$ for $\phi = 0.137$, $\alpha = 0.68$ for $\phi = 0.217$, and $\alpha = 0.70$ for $\phi = 0.404$. The magnitude of error in the stable measurement regime varied with the residual contrast of the damaged speckles C and the volume fraction of speckles in the image ϕ. In general, error improved with increasing ϕ and C. This was qualitatively consistent with the experiments, which also found that the high ϕ specimens exhibited a lower noise floor than low ϕ specimens.

Equivalent analysis on the strain error identified similar nonlinearities in the measurement precision, as revealed in Fig. 9. Specifically, the strain error increased linearly until a critical level of damage that was approximately identical to that identified in the displacement analysis. This transition point occurred at strain error of ≈0.0025 (250 $\mu\varepsilon$); this critical value (at $C = 0$) ranged from $\alpha = 0.48$ for $\phi = 0.137$, $\alpha = 0.60$ for $\phi = 0.217$, and $\alpha = 0.67$ for $\phi = 0.404$. Below this point, the strain error increased linearly with α. Again, the error decreased with larger ϕ and C.

Effect of Subset Size

Using the same synthetic tomograms (for $C = 0$), the DVC analysis was repeated to understand the effect of subset size on displacement error. These results are shown in Fig. 10, which highlight the stabilizing benefit of large subset size M on the DVC-measured displacement. These benefits were especially pronounced at low volume fractions: for $\phi = 0.137$, a displacement error of $\sigma_u = 0.25$ voxels was achieved at $\alpha = 0.47$ for $M = 21$ voxels, but at $\alpha = 0.78$ for $M = 31$ voxels. In contrast, with a denser speckle pattern of $\phi = 0.422$, the change in subset size from $M = 21$ to 31 voxels increased the DVC stability from $\alpha = 0.62$ to 0.88. Thus, an experimentalist can effectively adjust the subset size to compensate for speckle pattern degradation; of course, this benefit would also come at the cost of the measurement's spatial resolution.

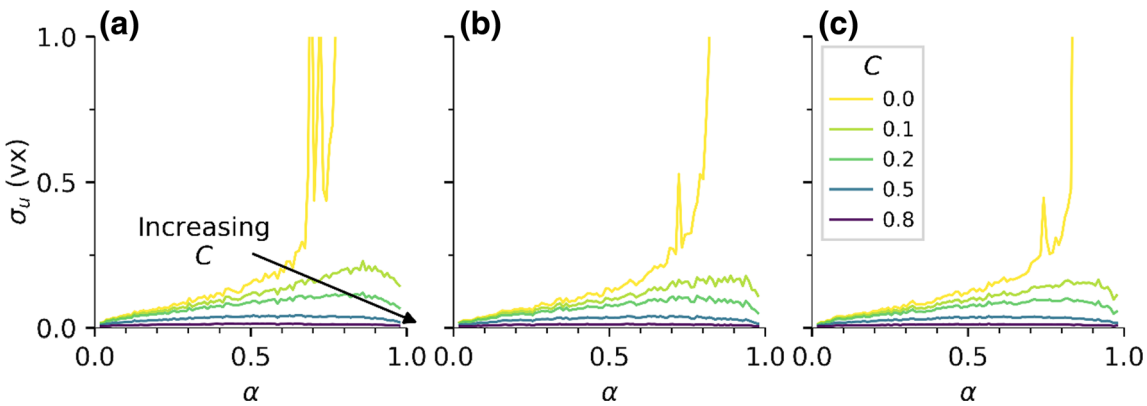

Fig. 8 Effect of speckle pattern degradation and volume fraction ϕ on displacement error. (a-c) Results for ϕ of (a) 0.137, (b) 0.217, and (c) 0.404. NSR = 3%

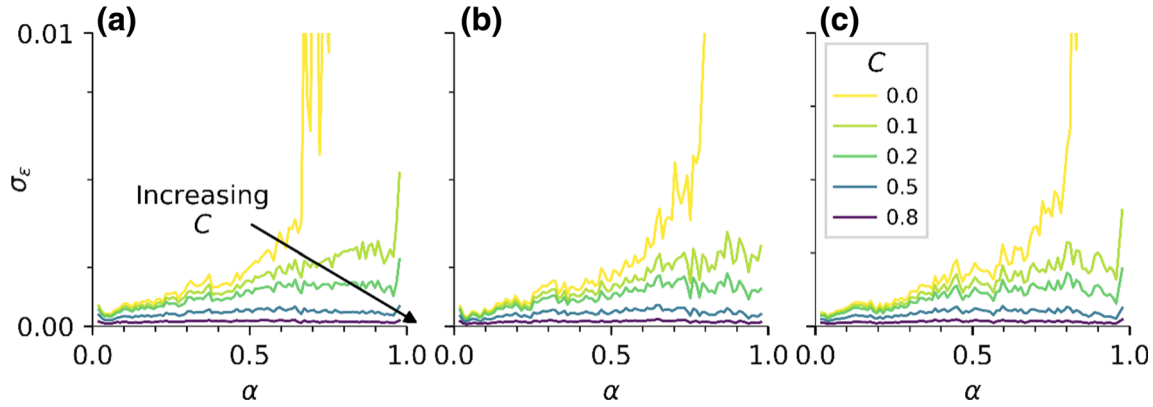

Fig. 9 Effect of speckle pattern degradation and volume fraction ϕ on strain error. (a-c) Results for ϕ of (a) 0.137, (b) 0.217, (c) 0.404. NSR = 3%

Theoretical Analysis

Predicting DVC Instability Due to Fragile Microstructures

The observed trends with regard to speckle pattern damage, subset size, and speckle volume fraction can be reconciled with existing theories of DIC/DVC error. Specifically, the following can be asserted:

- An increasing fraction of damaged speckles (α) will increase the mismatch between the reference and deformed subset, thereby increasing the DVC error.
- For constant α, a larger subset will retain more intact speckles in the deformed subset. Accordingly, the subset size M may be used to improve DVC accuracy in cases of pattern degradation.
- Similarly, a larger volume fraction ϕ of speckles will increase the number of intact speckles and improve measurement precision.

In the following section, these deductions are formalized in terms of the Sum of Subset Squared Image Gradients (SSSIG) criterion proposed by Pan [33]. In Pan's work, the DVC displacement error was quantitatively related to the image intensity gradients used for subvoxel interpolation in each subset. Ultimately, this analysis showed that the standard deviation of displacement error σ_{u_i} scales proportional to variance of the image noise $D(\eta)$ and inversely with SSSIG.

$$\sigma_{u_i} \propto \left(\frac{D(\eta)}{\sum_S \left(\frac{\partial G}{\partial x_i} \right)^2} \right)^{0.5} \tag{4}$$

where $\sum_S(\ )$ refers to a summation over all voxels in the subset, and G is the deformed tomogram with damaged speckles.

With some modification, the SSSIG criterion is shown to accurately predict the DVC instability associated with severe speckle pattern degradation for a variety of speckle patterns and DVC parameters. In this analysis, the results from subset-based sensitivity study described in the section "Effect of Subset Size" are used to demonstrate this behavior. Accordingly, their comparison is restricted to images with consistent speckle geometry, DVC step size, and image noise.

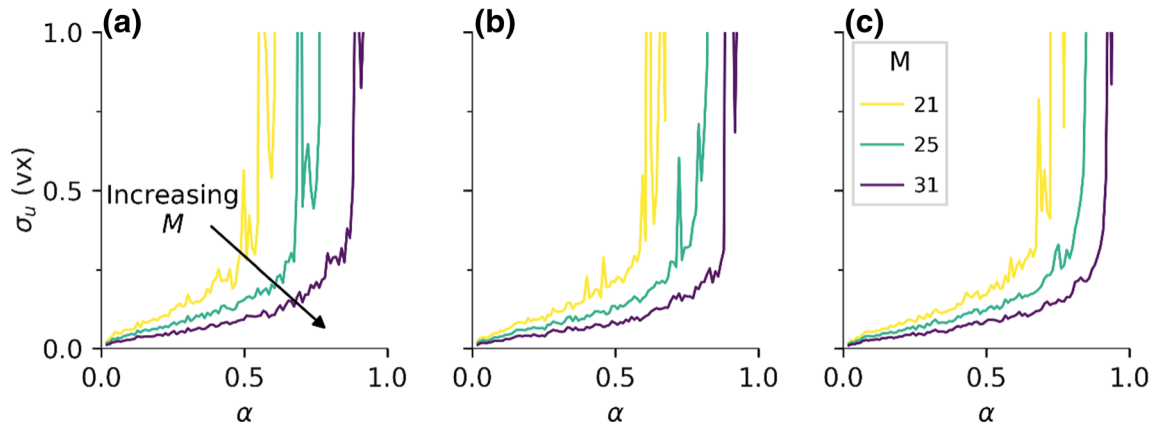

Fig. 10 Effects of subset size M on displacement error for ϕ of (a) 0.137, (b) 0.217, and (c) 0.404. $C = 0$, NSR = 3%

The analysis assumes that the images exhibit the following characteristics

- Uniform speckle size, shape and contrast, with non-overlapping speckles
- The average spacing of speckles can be characterized by a wavelength λ
- DVC analysis is performed with cubic subsets of size M
- Consistent, independent noise for each voxel

Given these conditions, SSSIG can be defined precisely by the number of intact speckles in each subset.

$$\sum_S \left(\frac{\partial G}{\partial x_i}\right)^2 = \mathcal{G}_i N_{intact} \tag{5}$$

where $N_{intact} = (1-\alpha)N_{speckles}$ and $N_{speckles} = \left(\frac{M}{\lambda}\right)^3$. $\mathcal{G}_i$ describes the individual contribution of each speckle to the SSSIG, $\mathcal{G}_i = \sum_s \left(\frac{\partial I_{speckle}(\boldsymbol{x})}{\partial x_i}\right)^2$, with $I_{speckle}$ as defined in Eq. 2 above.

Under this model, the DVC displacement error should scale inversely with N_{intact} for all combinations of M and ϕ (which is interchangeable with λ). This is tested in Fig. 11, which indeed reveals a consistent transition point between "stable" and "unstable" DVC measurement errors based on N_{intact}. Specifically, σ_u increased linearly until $N_{intact} = 11 - 20$ speckles, and increased rapidly for subsequent deletion of speckles. This threshold was valid for the wide range of $N_{speckles}$ from 26 and 150 in the undamaged state, and no obvious trends in the critical N_{intact} were identified with respect to either M or ϕ. As a result, it is postulated that this represents the minimum number of intact features for accurate DVC analysis.

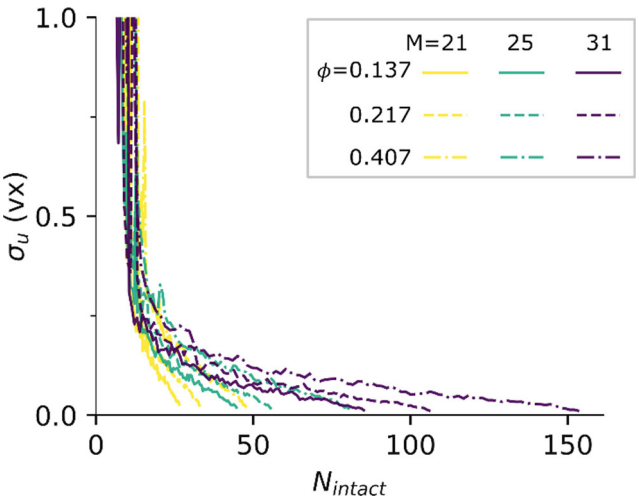

Fig. 11 Normalized model of DVC displacement error for different combinations of subset size M and volume fraction ϕ

Effect Of Damage on Correlation Strength

It is further speculated that the effects of damage on DVC error can be related to the correlation strength C_{ZNCC}. This is validated using two sets of 2D synthetic images of size 384^2 pixels (Fig. 12(a)), which were generated according to the methods described in the previous section Generation of Synthetic Images. In the first set, individual markers were damaged by a "fading" technique. In the second, the width of the markers was "shrunk" in proportion to the speckle damage. While both sets of images were identical in the undamaged and fully damaged states, the intermediate states were somewhat different. The undamaged images included a speckle fraction of $\phi = 0.26$. Half of the markers ($\alpha = 0.5$) were flagged for damage, while the other half of the speckles remained unchanged in the degraded images. The contrast C was reduced incrementally between images, which approximated the collapse of GMBs in the syntactic foam.

Results of the simulation in Fig. 12(b) indicated that the two damage mechanisms both reduced C_{ZNCC} nonlinearly.

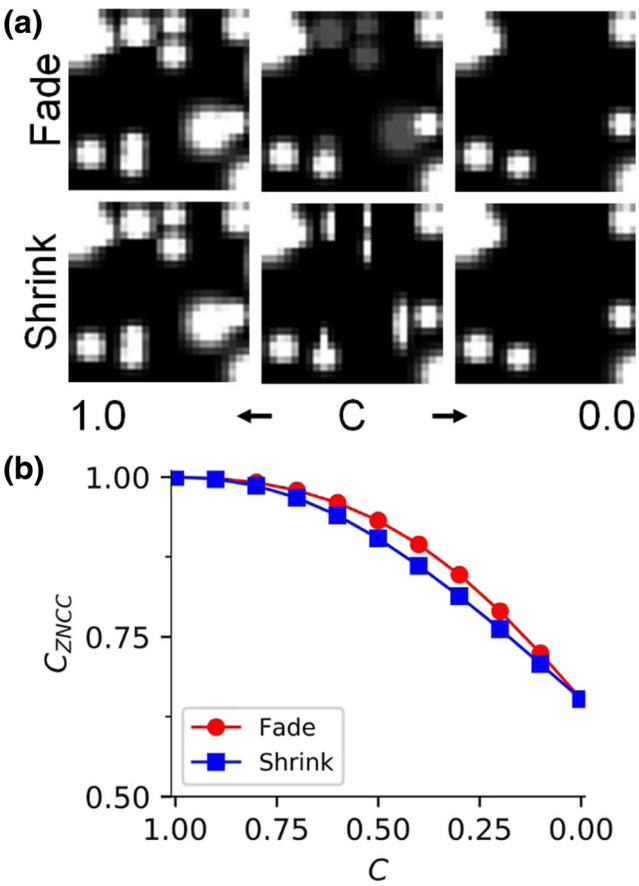

Fig. 12 Effect of "Fade" and "Shrink" speckle degradation mechanisms on DVC. (a) Schematic of the two mechanisms. (b) Resulting ZNCC scores as function of residual contrast C. $\alpha = 0.5$ of speckles were flagged for damage

Reductions in C_{ZNCC} can hinder local optimization schemes from successfully identifying the appropriate correlation peak [34, 35], leading to spurious displacement and strain measurements. Indeed, many commercial DIC and DVC software packages are configured to ignore subsets with poor correlation; in this case, severe decorrelation due to speckle pattern degradation would prevent any displacement measurement at all! Remarkably however, C_{ZNCC} remained above 0.9 for $C \geq 0.5$. While arbitrary, this threshold has been previously used to update the reference image in incremental DIC schemes and preserve measurement accuracy for large deformations [36, 37]. Given that the measurement accuracy scales with the correlation strength, it seems reasonable that DVC measurements could tolerate minor degradation to the speckle pattern, but become increasingly sensitive to subsequent damage.

Discussion

Comparison Between Experiment and Numerical Results

Most importantly, these results showed that accurate DVC measurements can be obtained despite non-trivial levels of degradation to the speckle pattern. This was confirmed using both experimental tomograms and numerically-generated images with controlled levels of speckle pattern degradation. In both cases, the DVC error remained small while below a critical level of degradation (*i.e.,* the stable measurement regime), after which the strain error rapidly increased to unacceptable levels (unstable measurement regime). Thus, the transition between stable and unstable measurement regimes reflected the degradation of the speckle pattern rather than peculiarities of the syntactic foams used in experiments. Fundamentally, this appeared to be related to the effects of speckle pattern degradation on the correlation strength C_{ZNCC}. The nonlinear dependence of C_{ZNCC} on degradation allowed C_{ZNCC} to remain high after the disappearance of a small fraction of speckles, but C_{ZNCC} rapidly decreased with further degradation.

Despite this, several key differences were observed between the two analyses. First, DVC error analysis of the experimental and numerically-generated images revealed different trends within the stable measurement regime. In particular, the experimental results suggested a constant error of $\sigma_u = 0.025 - 0.05$ *voxels* and $\sigma_\varepsilon = 50 - 100$ $\mu\varepsilon$ for all levels of degradation beneath the critical value, while the numerical images suggested a *linearly increasing* error within this range (for constant C). The likely explanation of this trend was that the effective C for the collapsed GMBs was not constant but decreased throughout the experiment. Initially, the Feret shape of damaged particles would be small, such that the particle would be pseudo-spherical and would provide strong residual contrast C in the tomogram. Subsequent loading would further compress the particles, increasing Feret shape and decreasing C. At small deformations, the typical C would remain large enough to negligibly affect the error. For example, from Figs. 8 and 9 it was shown that displacement or strain error did not substantially increase with $C \approx 0.5$ regardless of the fraction of speckles damaged. This allowed error to remain low when the GMBs were partially collapsed, but to rapidly increase as the damaged particles fully closed.

Second, analysis of the numerically-generated images predicted critical damage levels that were higher than those observed in the experiment. Plausibly, damage localization in the experiment contributed to the increased error. Detailed analysis of the tomograms showed that bands of elevated strain (visible in Fig. 5) corresponded to regions with clusters of crushed GMBs, such the speckle pattern damage would locally exceed the global average and therefore increase the measurement error. This behavior was caused by particle-to-particle interactions [38] and local clustering of GMBs [26], and was particularly severe in the high volume fraction specimens ($\phi = 0.422$ and to a lesser extent $\phi = 0.225$).

Implications

The ability to accurately correlate heavily damaged speckle patterns should enable DVC-based strain measurements in a broad class of materials with fragile microstructures, including syntactic foams and possibly many other materials. This was previously thought to be impossible or ill-advised at best, since it would violate the principle of gray-level conservation. In contrast, our experimental results showed that roughly 30–40% of speckles could disappear before strain error noticeably worsened to $\sigma_\varepsilon > 0.01$. Intriguingly, adjusting the subset size may be a viable technique to enable accurate DVC measurements in cases of even more severe degradation. In particular, analysis of the simulated images suggested that DVC analysis remained stable as long as each subset contained a minimum of $N_{intact} = 20$ speckles. In any case, rigid body motion experiments are essential to assess the error due to speckle pattern degradation, and should be included in any experimental protocol where results may be affected by microstructural damage.

The current findings were only obtained for particle-based speckle patterns, where damage resulted in the disappearance of particles in the pattern. Therefore, it remains unclear how other types of speckle patterns and damage mechanisms affect the stability of DVC measurements. Future work is required to assess this behavior in granular, foam or fibrous composites, and also materials that undergo different damage mechanisms such as microcracking or cell collapse. Simulation of these effects using numerically

generated images may prove a cost-effective manner to test viability of DVC measurement in these other materials.

Finally, these results demonstrate the importance of restricting DVC measurement to scenarios with sub-critical levels of speckle pattern degradation. For the current syntactic foam, this was achieved by relating damage to the uniaxial deformation, which was found to reliably correspond to DVC error across multiple samples with identical GMB volume fractions. Similar testing should be performed on other materials to avoid inaccurate strain measurements. Alternatively, in the case of super-critical speckle pattern degradation, the spatial distribution of subsets with large strain error could be used to identify regions of severe microstructural damage.

It becomes more challenging to define the critical level of speckle pattern degradation when damage is locally concentrated rather than homogeneously dispersed throughout the material, which would cause DVC error to increase more rapidly near the location of damage. While a straightforward but cautious approach would be to manually trim the region of interest around the damaged regions, this can be tedious and also disposes of many accurate correlation points. Since the speckle pattern degradation reduces the correlation strength, it may be possible to introduce automatic screening of each correlated subset. One intriguing avenue for evaluating the quality of the experimental strain measurement is to implement so-called q-factor DVC, which assesses the sharpness and uniqueness of the cross-correlation through image quality factors [35]. Q-factor DVC was originally developed for cases of large deformation, which causes round speckles to collapse into ellipses and is comparable to the collapse of GMBs in the syntactic foam. Additionally, this work can be integrated into the framework for incremental DIC/DVC techniques [36, 37] to indicate when the reference image should be updated.

Conclusions

Accurate DVC measurements were obtained during *in situ* testing of specimens with fragile microstructures even with widespread damage to the speckle pattern. This was validated using experiments on three types of syntactic foams with different volume fractions of glass microballoon reinforcement, as well as analysis of numerically-generated images with controlled levels of speckle pattern degradation; in both cases, correlation succeeded despite large proportions of individual markers in the speckle pattern disappearing between the reference and deformed states up to 20–35% compression and 30–40% damaged speckles. These findings justify the use of DVC on many types of materials with unstable or fragile microstructures, including syntactic foams, ceramic composites, bone and others. From these analyses, the following conclusions are made:

- The performance of DVC as a function of speckle pattern degradation was classified into two regimes. Below a critical level of speckle degradation, the DVC measurement was “stable” and the error approached the experimental noise floor. The displacement and strain errors were constant within this regime, and varied inversely with the speckle pattern density. Above this critical value, the measurement became “unstable” and the error rapidly increased with further degradation to the speckle pattern.
- In the experiments, the transition from stable to unstable measurement regimes typically occurred after 30–40% of the speckles were damaged. This critical value depended on several factors including pattern quality, marker volume fraction and the degree of damage localization. In particular, larger volume fractions of markers tended to stabilize the DVC measurements to accommodate more severe damage to the speckle pattern.
- The experimental trends were qualitatively replicated using numerically-generated images, which successfully captured the transition between stable and unstable measurement regimes. However, the numerical analysis tended to overestimate transition between these two regimes, likely due to subtle differences in the damage mechanisms between the syntactic foam and the simulated images. Despite this, numerically-generated images may be used to preliminarily simulate the viability of DVC measurements in other types of fragile speckle patterns, such as those found in foams or fiber-reinforced composites.
- The effect of damage on measurement error was reconciled with the Sum of Subset Squared Image Gradients (SSSIG) criterion proposed by Pan [33]. Using numerically generated images, the displacement error was shown to scale inversely with the number of intact N_{intact} speckles in each subset, and the DVC instability was triggered at roughly constant N_{intact} for a variety of speckle patterns and DVC parameters. As an implication, larger subset sizes may be used to compensate for sparse speckle patterns or severe pattern degradation.

Acknowledgements This research is supported by Sandia National Laboratories and the National Science Foundation (NSF) Graduate Research Fellowship Program (DGE-1842490). Sandia National Laboratories is a multimission laboratory managed and operated by National Technology and Engineering Solutions of Sandia, LLC., a wholly owned subsidiary of Honeywell International, Inc., for the U.S. Department of Energy’s National Nuclear Security Administration under contract DE-NA-0003525. This paper describes objective technical results and analysis. Any subjective views or opinions that might be expressed in the paper do not necessarily represent the views of the U.S. Department of Energy or the United States Government.

References

1. Sutton MA, Wolters W, Peters WH et al (1983) Determination of displacements using an improved digital correlation method. Image Vis Comput 1:133–139. https://doi.org/10.1016/0262-8856(83)90064-1
2. Bay BK, Smith TS, Fyhrie DP, Saad M (1999) Digital volume correlation: Three-dimensional strain mapping using X-ray tomography. Exp Mech 39:217–226. https://doi.org/10.1007/BF02323555
3. Sutton MA, Orteu J-J, Schreier HW (2009) Image Correlation for Shape, Motion and Deformation Measurements. Springer US, Boston
4. Dong YL, Pan B (2017) A Review of Speckle Pattern Fabrication and Assessment for Digital Image Correlation. Exp Mech 57:1161–1181. https://doi.org/10.1007/s11340-017-0283-1
5. Bay BK (2008) Methods and applications of digital volume correlation. J Strain Anal Eng Des 43:745–760. https://doi.org/10.1243/03093247JSA436
6. Croom BP, Xu P, Lahoda EJ et al (2017) Quantifying the three-dimensional damage and stress redistribution mechanisms of braided SiC/SiC composites by in situ volumetric digital image correlation. Scr Mater 130:238–241. https://doi.org/10.1016/j.scriptamat.2016.12.021
7. Saucedo-Mora L, Lowe T, Zhao S et al (2016) In situ observation of mechanical damage within a SiC-SiC ceramic matrix composite. J Nucl Mater 481:13–23. https://doi.org/10.1016/j.jnucmat.2016.09.007
8. Saucedo-Mora L, Mostafavi M, Khoshkhou D et al (2016) Observation and simulation of indentation damage in a SiC-SiCfibre ceramic matrix composite. Finite Elem Anal Des 110:11–19. https://doi.org/10.1016/j.finel.2015.11.003
9. Mazars V, Caty O, Couégnat G et al (2017) Damage investigation and modeling of 3D woven ceramic matrix composites from X-ray tomography in-situ tensile tests. Acta Mater 140:130–139. https://doi.org/10.1016/j.actamat.2017.08.034
10. Bouterf A, Maire E, Roux S et al (2018) Analysis of compaction in brittle foam with multiscale indentation tests. Mech Mater 118:22–30. https://doi.org/10.1016/j.mechmat.2017.12.004
11. Barhli SM, Saucedo-Mora L, Jordan MSL et al (2017) Synchrotron X-ray characterization of crack strain fields in polygranular graphite. Carbon N Y 124:357–371. https://doi.org/10.1016/J.CARBON.2017.08.075
12. Hild F, Bouterf A, Roux S (2015) Damage measurements via DIC. Int J Fract 191:77–105. https://doi.org/10.1007/s10704-015-0004-7
13. Valle V, Bokam P, Germaneau A, Hedan S (2018) New Development of Digital Volume Correlation for the Study of Fractured Materials. Exp Mech:1–15. https://doi.org/10.1007/s11340-018-0415-2
14. Rannou J, Limodin N, Réthoré J et al (2010) Three dimensional experimental and numerical multiscale analysis of a fatigue crack. Comput Methods Appl Mech Eng 199:1307–1325. https://doi.org/10.1016/J.CMA.2009.09.013
15. Roux S, Hild F, Viot P, Bernard D (2008) Three-dimensional image correlation from X-ray computed tomography of solid foam. Compos Part A Appl Sci Manuf 39:1253–1265. https://doi.org/10.1016/j.compositesa.2007.11.011
16. Bouterf A, Roux S, Hild F et al (2014) Digital volume correlation applied to X-ray tomography images from spherical indentation tests on lightweight gypsum. Strain 50:444–453. https://doi.org/10.1111/str12101
17. Pierron F, McDonald SA, Hollis D et al (2013) Comparison of the mechanical behaviour of standard and auxetic foams by x-ray computed tomography and digital volume correlation. Strain 49:467–482. https://doi.org/10.1111/str.12053
18. Verhulp E, van Rietbergen B, Huiskes R (2004) A three-dimensional digital image correlation technique for strain measurements in microstructures. J Biomech 37:1313–1320. https://doi.org/10.1016/j.jbiomech.2003.12.036
19. Forsberg F, Siviour CR (2009) 3D deformation and strain analysis in compacted sugar using x-ray microtomography and digital volume correlation. Meas Sci Technol 20:095703. https://doi.org/10.1088/0957-0233/20/9/095703
20. Bornert M, Lenoir N, Bésuelle P et al (2010) Discrete and continuum analysis of localised deformation in sand using X-ray μCT and volumetric digital image correlation. Géotechnique 60:315–322. https://doi.org/10.1680/geot.2010.60.5.315
21. Croom BP, Jin H, Mills B et al (2019) Damage mechanisms in elastomeric foam composites: Multiscale X-ray computed tomography and finite element analyses. Compos Sci Technol 169:195–202. https://doi.org/10.1016/j.compscitech.2018.11.025
22. Croom B, Wang W-M, Li J, Li X (2016) Unveiling 3D Deformations in Polymer Composites by Coupled Micro X-Ray Computed Tomography and Volumetric Digital Image Correlation. Exp Mech 56:999–1016. https://doi.org/10.1007/s11340-016-0140-7
23. Patterson BM, Escobedo-Diaz JP, Dennis-Koller D, Cerreta E (2012) Dimensional quantification of embedded voids or objects in three dimensions using X-ray tomography. Microsc Microanal 18:390–398. https://doi.org/10.1017/S1431927611012554
24. Patterson BM, Cordes NL, Henderson K et al (2016) In situ X-ray synchrotron tomographic imaging during the compression of hyper-elastic polymeric materials. J Mater Sci 51:171–187. https://doi.org/10.1007/s10853-015-9355-8
25. Gupta N, Kishore WE, Sankaran S (2001) Studies on compressive failure features in syntactic foam material. J Mater Sci 36:4485–4491. https://doi.org/10.1023/A:1017986820603
26. Yu M, Zhu P, Ma Y (2013) Effects of particle clustering on the tensile properties and failure mechanisms of hollow spheres filled syntactic foams: A numerical investigation by microstructure based modeling. Mater Des 47:80–89. https://doi.org/10.1016/j.matdes.2012.12.004
27. Croom BP, Jin H, Carroll J et al (2018) Particle clustering effects on damage mechanisms in syntactic foams. Submitted
28. Adrien J, Maire E, Gimenez N, Sauvant-Moynot V (2007) Experimental study of the compression behaviour of syntactic foams by in situ X-ray tomography. Acta Mater 55:1667–1679. https://doi.org/10.1016/j.actamat.2006.10.027
29. Limodin N, Réthoré J, Adrien J et al (2011) Analysis and Artifact Correction for Volume Correlation Measurements Using Tomographic Images from a Laboratory X-ray Source. Exp Mech 51:959–970. https://doi.org/10.1007/s11340-010-9397-4
30. Mazzoleni P, Matta F, Zappa E et al (2015) Gaussian pre-filtering for uncertainty minimization in digital image correlation using numerically-designed speckle patterns. Opt Lasers Eng 66:19–33. https://doi.org/10.1016/j.optlaseng.2014.08.004
31. Lachambre J, Maire E, Adrien J, Choqueuse D (2013) In situ observation of syntactic foams under hydrostatic pressure using X-ray tomography. Acta Mater 61:4035–4043. https://doi.org/10.1016/j.actamat.2013.03.017
32. Gupta N (2007) A functionally graded syntactic foam material for high energy absorption under compression. Mater Lett 61:979–982. https://doi.org/10.1016/j.matlet.2006.06.033
33. Pan B, Xie H, Wang Z et al (2008) Study on subset size selection in digital image correlation for speckle patterns. Opt Express 16:7037. https://doi.org/10.1364/OE.16.007037
34. Pan B, Qian K, Xie H, Asundi A (2009) Two-dimensional digital image correlation for in-plane displacement and strain measurement: a review. Meas Sci Technol 20:062001. https://doi.org/10.1088/0957-0233/20/6/062001

35. Landauer AK, Patel M, Henann DL, Franck C (2018) A q-Factor-Based Digital Image Correlation Algorithm (qDIC) for Resolving Finite Deformations with Degenerate Speckle Patterns. Exp Mech 58:815–830. https://doi.org/10.1007/s11340-018-0377-4
36. Pan B, Dafang W, Yong X (2012) Incremental calculation for large deformation measurement using reliability-guided digital image correlation. Opt Lasers Eng 50:586–592. https://doi.org/10.1016/j.optlaseng.2011.05.005
37. Hu Z, Luo H, Bardenhagen SG et al (2015) Internal Deformation Measurement of Polymer Bonded Sugar in Compression by Digital Volume Correlation of In-situ Tomography. Exp Mech 55:289–300. https://doi.org/10.1007/s11340-014-9856-4
38. Tagliavia G, Porfiri M, Gupta N (2011) Analysis of particle-to-particle elastic interactions in syntactic foams. Mech Mater 43:952–968. https://doi.org/10.1016/j.mechmat.2011.08.008